Available online at www.sciencedirect.com
SCIENCE DIRECT®
ELSEVIER
International Journal of Solids and Structures 42 (2005) 1943–1955
INTERNATIONAL JOURNAL OF SOLIDS and STRUCTURES
www.elsevier.com/locate/ijsolstr

A shape memory-based multifunctional structural actuator panel

Dana M. Elzey *, Aarash Y.N. Sofla, Haydn N.G. Wadley

Department of Materials Science & Engineering, University of Virginia, 116 Engineer's Way, P.O. Box 400745, Charlottesville, VA 22904-4745, USA

Received 27 April 2004

Abstract

A multifunctional panel concept is presented in which a lightweight, structurally efficient sandwich panel is able to undergo a reversible change in shape upon application of a localized thermal stimulus while supporting significant load. The shape change is effected by shape memory alloy face sheet elements, which exploit a "one-way" shape memory effect only. Unlike other related designs, no external or bias forces are required to complete the full cycle of shape change. The reversible shape change is accomplished by a core design which forces an inactive face sheet to martensitically deform in tension when the opposing face sheet undergoes a length change. By alternately heating one face sheet and then the other, the sandwich panel is able to perform fully reversible cyclic shape changes. The performance of the sandwich panel, in terms of required thermal power, actuation frequency, peak load bearing capacity, stiffness, and weight, can be optimized by proper selection of face sheet material and its thickness, the overall core thickness, core member thickness and length, and the design of the joint connecting core members and face sheet.

Keywords: Shape memory alloy; Actuator; Multifunctional; Ni–Ti; Sandwich panel; Cellular metals; Phase transformation

1. Introduction

New multifunctional materials concepts for lightweight, load bearing structures capable of controlled, reversible shape changes are needed for a wide range of aerospace, robotics and other applications (Garcia, 2002). Such shape-morphing structural elements are potential replacements for existing systems relying on separate structural and actuation components. Examples include hydraulically actuated wing flaps and undersea vehicle rudders for ships and submersed vehicles. This paper discusses the development, testing and analysis of a reversible, shape-morphing structural element which relies on a shape memory alloy for actuation. Shape memory alloys (SMA) have been extensively applied in micro-electro-mechanical systems (MEMS) (Srinivasan and McFarland, 2001), surgical devices (Flomenblit et al., 1994) and prostheses as

* Corresponding author. Tel.: +1-434-9825796; fax: +1-434-9825660/799.
E-mail address: dme2j@virginia.edu (D.M. Elzey).

0020-7683/$ - see front matter © 2004 Elsevier Ltd. All rights reserved.
doi:10.1016/j.ijsolstr.2004.05.034

well as smart materials concepts (Schetky, 1998) pertinent to the work described here. SMA, such as those based on Ni–Ti and Cu–Zn–Al, rely on a martensitic phase transformation to absorb inelastic strains (as high as 5–8%). Heating above the austenite start transformation temperature enables the material to recover its original shape (Otsuka and Wayman, 1998). The spontaneous return of a deformed SMA sample to its original shape (or dimensions) upon heating is referred to as the one-way shape memory effect. A two-way effect is also possible, in which the SMA cycles between two fixed shapes during cycling between an upper and lower transformation temperature (Otsuka and Wayman, 1998). Interested readers may find more on the structure, composition and constitutive behavior of SMA from the literature (Otsuka and Wayman, 1998; Fu et al., 2001; Saburi, 2000).

Most SMA-based actuators operate cyclically between two states and so, if based on the one-way effect, require a biasing force (such as a spring) to return the SMA to its low-temperature (martensitic) shape. Such designs are inefficient because the work provided by the shape recovery is partitioned between the bias element, that is stored (elastically) in the structure, and that available to do work against applied loads (the useful part). Lu et al. (2001) have recently proposed and analyzed a lightweight, shape-morphing sandwich panel incorporating a single SMA face sheet bonded to a truss core. Their design is based on a two-way shape memory effect, in which one shape is acquired at the upper transformation (austenite finish, A_f) temperature and another shape at the lower transformation (martensite finish, M_f) temperature. Using a statically determinate core design, they are also able to minimize storage of elastic strain energy in the core and therefore achieve greater efficiency. This concept is difficult to implement for many applications however, due to extremely low transformation forces upon cooling and the relatively small ($<2\%$) length change available via the two-way effect (Otsuka and Wayman, 1998). In a‘ second approach, Lu et al. have proposed the use of a single face sheet, one-way SMA actuator that uses a bias force to restore the structure to its original configuration (Lu et al., 2002). While a more practical strategy, it is less efficient because of the need to store energy in the mechanical structure used to cause the shape reversal.

Here, we describe the design of a lightweight, shape-reversing structural panel (or beam element) which requires no bias force and relies on a one-way shape memory effect only. The concept is based on a face sheet-stiffened sandwich panel, in which both face sheets are made of a one-way SMA. These are bonded or attached to a truss core that has a very low resistance to bending, combined with a high resistance to in-plane shear. The design is such that, when one of the two face sheets is heated to the A_f temperature, the other (low-temperature) face is subjected to deformation by the formation of stress-induced martensite. A prototype has been constructed using Ni–Ti SMA face sheets bonded to a stainless steel truss core. While the face sheets deform inelastically via the formation of stress-induced martensite, the core experiences only elastic deformations. The shape is reversed by heating the opposite face sheet to A_f, and cycled at a frequency determined by the rate at which the face sheets cool after heating. We expect this approach to result in reversible shape actuator panels with performance comparable to designs using an external bias mechanism, but at lower system weight, resulting in improved structural efficiency. A further advantage of the design considered here is its ability to maintain its actuated shape with no power input.

2. Design concept

Fig. 1(a) shows a schematic illustration of the actuator panel concept, consisting of SMA face sheets bonded to a stainless steel truss core. Heating of the SMA face sheets can be achieved by Joule (direct electrical resistance) heating, by radiative mechanisms, or by flow of a heated gas or liquid over one or the other sheets. The central core sheet separates these flows from the opposite face sheet. A 2D model core is constructed by forming corrugated sheets which are then transient liquid phase bonded to both sides of the flat (stainless steel) core sheet. Geometric design variables include the face sheet thickness, t_f, truss member

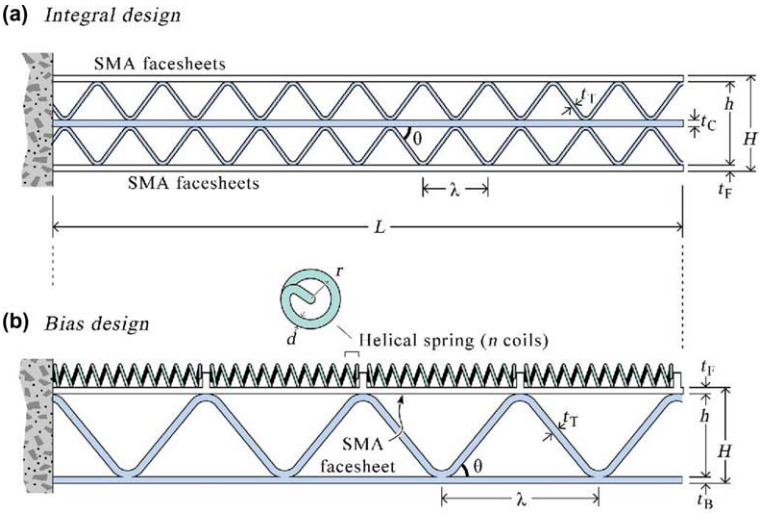

Fig. 1. (a) Design concept for a two-way, shape-reversing, structural element based on a one-way shape memory material (integral), (b) bias design using elastic springs to provide shape-reversing capability.

thickness, t_t, core sheet thickness, t_c, truss angle, θ, total core thickness, H, and beam length, L. The core, which consists of a series of reinforced diamond truss elements, has the desired attributes of low density, low bending stiffness (until faces are attached), and high in-plane shear strength.

The as-received SMA face sheets, prior to attachment to the core, are first heated above their A_f temperature to ensure the material is in its austenitic form. This is followed by uniaxial elongation to roughly half the alloy's expected shape memory strain (3–4% for Ni–Ti SMA). The direction of elongation will be referred to as the longitudinal direction of the face sheet. The face sheets are then oriented so the longitudinal direction is perpendicular to the core's corrugations, and attached to the core, which is held in its flat, neutral configuration (i.e. the panel has no overall curvature).

If the upper face sheet is then heated to its austenite start temperature (A_s), it begins to contract, recovering the previously imposed tensile elongation as the temperature approaches A_f. The heated face sheet is referred to as the *active* face sheet, the unheated face as the *inactive* face sheet. The core is designed such that, as the active face sheet contracts in the longitudinal direction, an equal, but opposite (tensile) deformation is imposed upon the inactive face sheet. Since the yield strength of the austenitic phase is much greater (roughly a factor of three in the case of Ni–Ti) than the stress required to induce the martensitic transformation in the inactive face sheet (Mellor, 1987), the inactive face further elongates to nearly its full expected shape memory strain. Since the core is designed to resist in-plane shear (i.e. to withstand the force required to deform the inactive face sheet), contraction of the active face causes the panel to become curved, with the active face sheet towards the center of curvature. Once the active face sheet has cooled to below the austenite start temperature, the opposite face sheet is heated to A_f, causing the panel to reverse its curvature. Alternate heating and cooling of the face sheets thus allows the panel to be cycled between the two shapes as shown in Fig. 2. The frequency of cycling is limited by the rate of cooling of the active face sheet in the case of natural cooling, but could be accelerated by forced cooling, and as pointed out by Bart-Smith (2001), by arranging for the face sheet's quiescent temperature to be close to A_s. Whereas bias designs require a constant input of power to maintain their actuated shape, the integral reversing actuator described here maintains either limiting shape indefinitely with no power input. This holds true even under an externally imposed loading so long as stresses in the SMA component remain below the yield strength of the low-temperature phase.

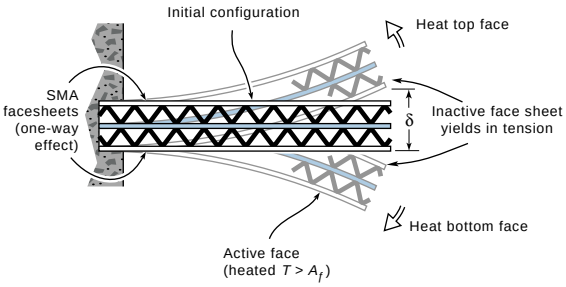

Fig. 2. Alternate heating (and cooling) of the SMA face sheets enables the structural actuator to cyclically reverse shape between two limiting configurations.

Optimal performance is obtained by maximizing the shape change or actuation force, and/or cycling frequency of the panel, while minimizing total weight. Gibson and Ashby (1997) cite the constraints on the design of such sandwich structures, namely that they must not fail due to buckling or plastic yielding (of face sheet, core sheet or truss member). An analysis of these performance attributes is developed in the following section and applied to identify useful design guidelines. These results are then compared with experimental results in Section 4.

3. Analysis

The shape-morphing structural panel described above must be able to perform useful work against specified loads, displacements (or curvature) and displacement rates. The optimal design will satisfy these performance requirements at the lowest weight and power consumption. It may also be required that the structure be able to cycle its shape at a specified minimum frequency. An analysis of the structure illustrated in Fig. 1(a) is developed to address such design issues. The analysis considers a cantilever beam of length, L, overall height, H, and width, B.

3.1. Actuator displacement

When the top face of the cantilever beam shown in Fig. 1(a) is heated to A_f, the face will contract by an amount given by $\Delta L = \varepsilon_{\alpha\beta}L/2$, where $\varepsilon_{\alpha\beta}/2$ is one-half the achievable shape memory strain for the specified SMA. As the top face contracts, the bottom face sheet is deformed in tension by the same amount (provided the core material is stiff and core failure does not occur). The stress needed to deform the bottom (inactive) face sheet is given by $\sigma_{\alpha\beta}$—this is the austenite (β) to martensite (α) transformation stress schematically illustrated in Fig. 3. The core, including the central core sheet, remains undeformed (except for elastic strains, which are much smaller than $\varepsilon_{\alpha\beta}$), and so, with no externally applied forces, the beam's curvature, $\kappa = 2\varepsilon_{\alpha\beta}/H$. From the geometry, the tip displacement in the absence of an applied load is

$$\delta_0 = \frac{H}{2\varepsilon_{\alpha\beta}}\left(1 - \cos\frac{2\varepsilon_{\alpha\beta}L}{H}\right) \tag{1}$$

Eq. (1) approximates reasonably well to $\delta_0 \approx \varepsilon_{\alpha\beta}L^2/H$, for $H/L > 0.1$, from which it is seen that the actuator displacement is increased by designing thinner, longer beams from SMA face sheets having a high transformation strain.

If a transverse external load, F, is applied to the end of the beam (as shown in Fig. 4), the tip displacement is $\delta \approx \delta_0 - \delta_F$, where δ_F is the forced displacement, consisting of shear and bending terms.

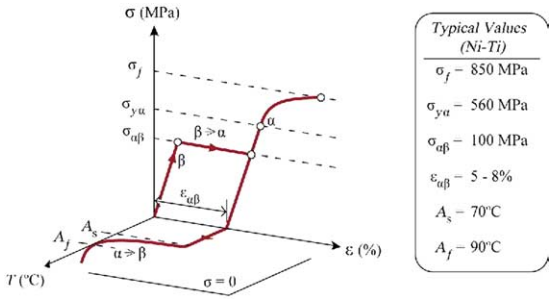

Fig. 3. Stress–strain–temperature plot illustrating the one-way shape memory effect in the Ni–Ti SMA. At room temperature, stressing to $\sigma_{\alpha\beta}$ results in perfectly plastic behavior while the austenite phase (β) transforms to martensite (α). A plastic "shape memory" strain ($\varepsilon_{\alpha\beta}$) remains after unloading. Heating to the austenite start temperature (A_s) and to A_f, the austenite finish temperature results in reversion of martensite to austenite and a consequent recovery of the shape memory strain. See Otsuka and Wayman (1998) for details.

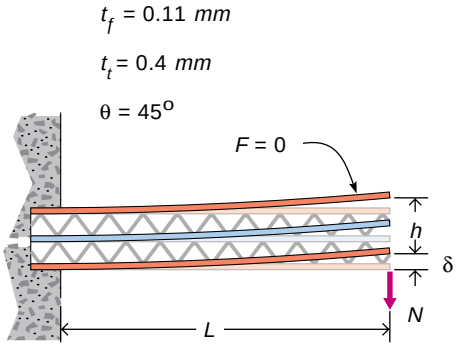

Fig. 4. The tip displacement of the actuator in cantilever beam configuration is given as the actuated displacement minus the deflection due to an externally applied force, F.

Normalizing by the length, L, and substituting appropriate expressions for δ_F (e.g. see Gibson and Ashby, 1997; Allen, 1969) leads to the normalized tip displacement for an arbitrary load, F:

$$\frac{\delta}{L} = \varepsilon_{\alpha\beta}\left(\frac{H}{L}\right)^{-1} - \left(\frac{2F}{3Bt_f E_f H^2}\left(\frac{H}{L}\right)^{-2} + \frac{F}{2Bt_t E_c \sin^2\theta\cos\theta}\right) \tag{2}$$

This analysis is valid assuming $t_f/H \ll 1$ and that the bending stiffness of the core alone is negligible, so that the flexural rigidity is dominated by the bending moment of the faces about the centroid of the sandwich beam.

Eq. (2) can be used to find the aspect ratio (H/L) providing the maximum displacement possible for a given applied load. (The core sheet and truss are taken to be the same material, so E_c is also the stiffness of the core sheet.) Fig. 5 illustrates the dimensionless tip displacement predicted by (2) as a function of the beam's aspect ratio (H/L) and the applied load (F). Failure (by face sheet yielding) occurs at higher beam aspect ratio with increasing applied load.

3.2. Input power requirement and peak cycling frequency

The reverse phase transformation (to the austenite parent phase) is quite rapid (at roughly the speed of sound in the material) once the recovery temperature has been reached. The frequency with which the

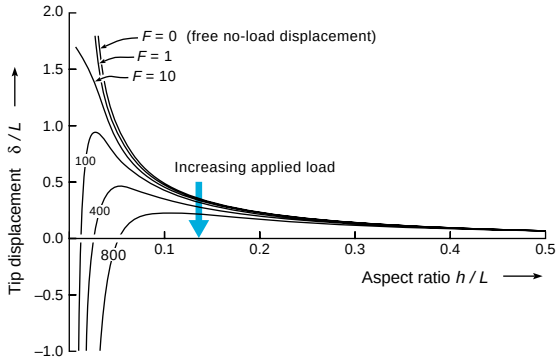

Fig. 5. Predicted displacement capacity as a function of beam geometry (aspect ratio, H/L) and applied force (units of N). Although not shown, increasing applied force at decreasing aspect ratio leads to failure of the element either by plastic yielding or elastic buckling.

structural SMA panel can alternate between its two limiting shapes is really dependent on the rate of heat transfer into and out of the SMA faces. We consider the case in which the SMA face sheets are heated resistively by directing current (I) through the sheets. The power (P) supplied is then $P = I^2R$, where R is the resistance in ohms. Also, it is assumed that the core is isolated from the face sheets, so that the core is not resistively heated and to minimize heat loss by conduction to the core. Following Lu et al. (2001), the governing heat transfer equation is

$$\rho_f c_p^f \frac{\partial T}{\partial t} = k_f \frac{\partial^2 T}{\partial x^2} - \frac{2\tilde{h}}{t_f}(T - T_0) + \sigma_\rho \left(\frac{I}{Bt_f}\right)^2 + \frac{\rho_f BLt_f \Theta}{\Delta t} \tag{3}$$

where ρ_f is the face sheet density, c_p is the specific heat capacity, k_f is thermal conductivity, $\tilde{h}$ is the surface heat transfer coefficient, σ_ρ is the resistivity, and Θ is the latent heat associated with the martensitic phase transformation. The terms on the RHS of Eq. (3) represent, from left to right, the energy absorbed in raising the face sheet temperature, losses to due convective heat transfer (radiative losses are neglected), energy supplied by Joule heating, and the latent heat of phase change. Eq. (3) can be simplified by observing that the latent heat term is negligible compared to the Joule heating term (Lu et al., 2001) and also by neglecting any heat loss through the face sheet's edges.

The solution to Eq. (3) leads to the frequency with which the temperature can be cycled between a lower limit, T_1, and an upper limit, T_2, is then

$$v = \frac{1}{2}\left\{\left(\ln\frac{(T_2 - T_0)}{(T_1 - T_0)}\right)\frac{T_1 - T_0 - \sigma_f\left(\frac{I}{Bt_f}\right)^2 \frac{t_f}{2\tilde{h}}}{T_2 - T_0 - \sigma_f\left(\frac{I}{Bt_f}\right)^2 \frac{t_f}{2\tilde{h}}}\right\}^{-1} \tag{4}$$

where T_0 is the initial temperature of the face at the start of the first cycle, T_1 is the initial temperature for subsequent cycles. The reader is referred to Lu et al. (2001) for intermediate solution steps. Using parameters in Table 1, the effect of increasing input current on the cycling frequency can be seen from Fig. 6; at high current input, the cycling frequency saturates due to the dominance of the cooling rate. Thinner face sheets allow the frequency of cycling to be increased.

Table 1
Model input parameters

Element	Property (symbol)	Value	Units
SMA (Ni–Ti) face sheet	Density (ρ_f)	6450	kg/m^3
	Austenite start temperature (A_s)	70 ± 5	
	Austenite finish temperature (A_f)	90 ± 5	
	Elastic modulus—high T (E_β)	85	GPa
	Elastic modulus—low T (E_α)	28	GPa
	SMA yield strength—high T ($\sigma_{y\beta}$)	500	MPa
	SMA yield strength—low T ($\sigma_{\alpha\beta}$)	100	MPa
	Shape memory strain ($\varepsilon_{\alpha\beta}$)	5	%
	Heat capacity (c_p)	500	J/kg K
	Heat transfer coefficient ($\tilde{h}$)	50	W/m K
	Resistivity (σ_f)	0.7	$\mu\Omega$ cm
Core (304 stainless steel)	Density (ρ_t)	7900	kg/m^3
	Elastic modulus (E_c)	200	GPa
Bias spring (high C steel)	Bias spring density (ρ_s)	7900	kg/m^3
	Shear modulus (E_s)	80	GPa

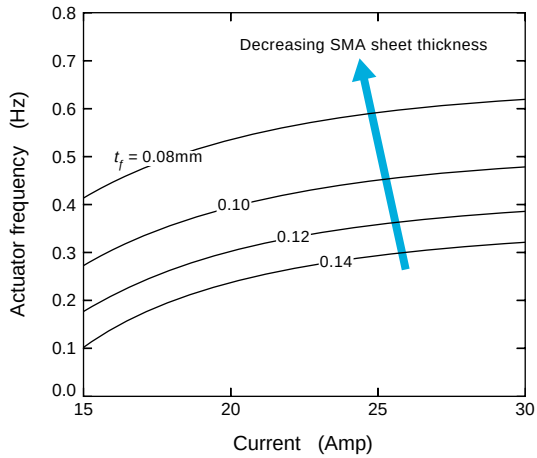

Fig. 6. Predicted panel shape cycling frequency as a function of input current. Thinner face sheets lead to increased operation frequency through increased heating and (natural) cooling rates.

4. Experimental

Several prototypes of the reversing actuator panel concept were built and tested. All of these have incorporated the 304 stainless steel core design illustrated in Fig. 1(a) . Strips of 0.5 in. (12.5 mm) width were cut from 0.016 in. (0.4 mm) sheet, then corrugated using a small brake. The corrugated stainless steel strips were then joined to both sides of a flat (304) strip using a transient liquid phase bonding process (Sypeck and Wadley, 2001). Early prototypes relied on a high strength epoxy adhesive to join the SMA face sheets to the truss core. While the polymer adhesive acted to insulate the core both electrically and thermally from the face sheets during actuation, it was found that the shear strength of the adhesive joint was insufficient, leading to premature failure.

The prototype tested here relies on an adhesive reinforced by threaded fasteners. The core was held in place by the adhesive while holes were marked and drilled (using a CNC milling machine) for the fasteners (two per 12.5 mm wide core–face joint). The Ni–Ti face sheets were prepared by cutting 0.5 in. (12.5 mm) × 4 in. (10 cm) strips from 0.0045 in. (0.11 mm) thick SMA sheet, and heating these to slightly above the A_f temperature (90 °C). This ensured the elimination of residual, stress-induced martensite. The next step attached the face sheets to the core. Two different approaches were tried; both were successful. The first method involved holding the core in a curved position (with a curvature approximating that which would be obtained during actuation of the completed panel), while the first face sheet was attached to the concave side. The core plus one face sheet was then bent (using a 3-point bend fixture designed for the purpose) until the fully *reversed* curvature was achieved. This elongated the attached face sheet and prepared it for contraction upon heating. Once the curvature had been reversed, the remaining face sheet (austenitic) was attached to the opposite side, which was then concave.

A second method (preferred) offers the advantage of allowing the face sheets to be attached to the core in a flat position. The heat treated strips were first mounted in a tensile test machine and elongated at room temperature to a 4% tensile strain (or approximately one-half the SMA's shape memory strain, $\varepsilon_{\alpha\beta}$). Extra material may be included for gripping, which can be afterwards trimmed prior to attachment with the core. Both face sheets were then attached to the core, which was held in a flat position. The panel could be actuated by heating either face sheet. Regardless of the attachment method, care must be taken not to heat both face sheets at once. Even if failure of the panel was avoided, the panel's actuation ability would be permanently impaired.

Prototypes prepared using both of the assembly processes described above have successfully demonstrated the two-way shape-reversing concept. Experimental data for tip displacement (in one direction) as a function of applied load are presented in Fig. 7. The SMA faces were heated using an insulated resistance heating element (wire) wound helically around the SMA. The load was applied by attaching a free weight to the end of the cantilever, and lifted upwards by activating (heating) the upper face sheet, as shown in Fig. 8. The length of the cantilever was 7.87 in. (200 mm), height 0.48 in. (12 mm) and width 0.48 in. (12 mm). The predicted tip displacement given by Eq. (2) is also shown, with the shape memory strain ($\varepsilon_{\alpha\beta}$) adjusted to optimize the intercept (i.e. the predicted zero-load displacement).

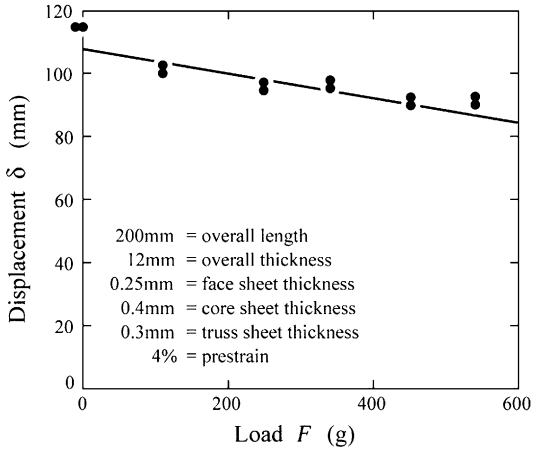

Fig. 7. Experimental (dots) versus predicted (Eq. (2)) cantilever beam actuator displacement (from a flat reference position) as a function of applied transverse load at the tip.

Fig. 8. Prototype (200 mm length) beam, fixed in vise at left, lifting 1.2 lb (540 g) a distance of 92 mm. The thermocouple shows temperature (°C) of the active (top) SMA face.

5. Discussion

A significant advantage of the current (integral) actuator design is its ability to achieve fully reversing shape change without the need for any bias (elastic restoring) force. Designs which incorporate a bias element (e.g. a coil spring) to reverse the actuator's shape have the disadvantages of not retaining their actuated shape unless power is supplied continuously to heat the SMA and the storage of elastic strain energy in the bias element and structure during actuation. While these comparisons are easily identified, it remains unclear which actuator design offers the most actuator force capability per unit weight. To explore this, we briefly develop dimensionless expressions for weight and load capacity for a cantilever beam of both designs and compare their maximum load capacity versus actuator weight.

The load which can be applied to the tip of a shape-actuated cantilever beam of either integral or bias design is determined by the limiting failure mechanism. The failure mechanisms for cellular metal beams, such as those shown in Fig. 1, include plastic yielding and elastic buckling of the faces, center sheet or trusses. Lu et al. (2001) have recently summarized the limiting loads for these failure mechanisms for a truss core sandwich beam design; these failure criteria have been rewritten for the two designs of interest here (see Fig. 1). The condition to avoid elastic buckling of the center sheet in the integral design is

$$\sigma_c = \frac{FL}{Bt_cH} \leqslant \frac{\pi^2}{8} E_c \left(\frac{t_c}{\lambda}\right)^2 \tag{5}$$

where F is the load applied transversely at the tip of the cantilever beam, E_c is the modulus for the core sheet material and other symbols refer to dimensions given in Fig. 1. Substituting for $\lambda(=2h/\tan\theta)$ and solving for t_c then gives

$$t_c \leqslant \sqrt[3]{\frac{8FLH}{\pi^2 E_c B \tan^2\theta}} \tag{6}$$

Given the overall actuator dimensions (B, L and H), Eq. (6) affords a means of specifying the core sheet thickness just sufficient to prevent buckling without the need to specify the other sheet thicknesses. By exploiting similar constraints on the thickness of the truss (t_t) and faces (t_f), the actuator's dimensions, and thus weight, are fully specified. The expressions for truss and face sheet thickness are

$$t_t \leqslant \sqrt[3]{\frac{3FH^2}{\pi^2 E_c B \sin\theta}} \tag{7}$$

to prevent buckling of the truss core and

$$t_f \leqslant \frac{2FL}{BH\sigma_{y\beta}} \tag{8}$$

to avoid plastic yielding of the SMA face sheet (in the high temperature [austenitic] state). With dimensions specified, the actuator's weight can now be determined using

$$W_i = BLt_c\rho_c + BL\frac{t_t}{\cos\theta}\rho_t + BLt_f\rho_f \tag{9}$$

where ρ_c, ρ_t and ρ_f are the center sheet, truss and face densities, respectively. Adopting the same notation used by Lu et al. (2001), we write the dimensionless weight index as

$$\Psi = \frac{W_i}{BL^2\rho_f} = \frac{1}{L}\left(t_c\frac{\rho_c}{\rho_f} + \frac{t_t}{\cos\theta}\frac{\rho_t}{\rho_f} + t_f\right) \tag{10}$$

The failure criteria (as given by Eqs. (6)–(8) for the integral actuator design) and the weight index (Eq. (10)) can now be used to plot the maximum load which can be supported by the actuator as a function of the beam's weight (Fig. 9). For comparison, we develop analogous expressions for the bias actuator design. The failure criteria are again used to write expressions for minimum face and truss sheet thickness to avoid buckling:

$$t_f \leqslant \sqrt[3]{\frac{128FLH}{\pi^2 E_c B \tan^2\theta}} \tag{11}$$

$$t_t \leqslant \sqrt[3]{\frac{12FH^2}{\pi^2 E_c B \sin\theta}} \tag{12}$$

The face sheet thickness to avoid plastic yielding is again given by Eq. (8). As for the integral design, a weight index is written as $\Psi = W_b/(BL^2\rho_f)$ with the weight, W_b, now given by

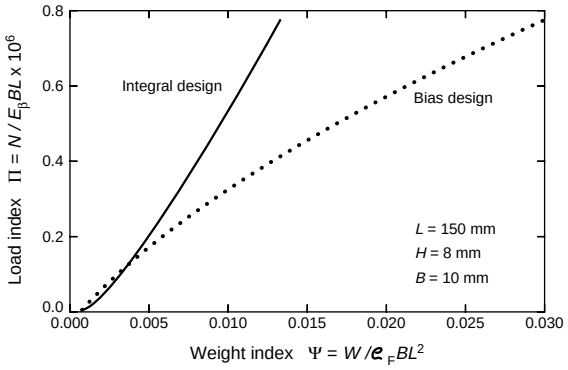

Fig. 9. Comparison of integral and bias design cantilever beam actuators—the weight penalty associated with the mechanical spring makes the bias design less efficient at high loads.

$$W_b = BLt_b\rho_t + \frac{BLt_t}{\cos\theta}\rho_t + BLt_f\rho_f + 2c\pi^2 nd^3\rho_s \tag{13}$$

where ρ_t is the density of the truss core material, and t_b, t_t and t_f are thicknesses of the base, truss and SMA face (see Fig. 1). The final term on the RHS of (13) represents the mass of the bias spring; c is the ratio of the coil spring radius (r) to wire diameter (d), i.e. $c = r/d$, and n is the number of coils in the spring. The spring's dimensions (as given by c and d), and the number of coils, n, determine the spring's mass and stiffness (N/mm). The basic design requirement for the bias spring is that it provide a force sufficient to deform the SMA face in its low-temperature state (i.e. $T < A_s$). This force is given by $f_{sma} = \sigma_{\alpha\beta}Bt_f$, where $\sigma_{\alpha\beta}$ is the stress required to deform the SMA at low temperature. The force–deflection relationship for a helical coil spring is (Baumeister et al., 1978)

$$F_s = \frac{Gd^4}{64nr^3}\delta \tag{14}$$

where G is the shear modulus of the material of which the spring is made and δ is the deflection. We let the deflection of the spring in the initial actuator configuration (i.e. flat, as pictured in Fig. 1) be δ_0, and the deflection when fully actuated (beam deflects upward as SMA face contracts) be δ_c. Since the spring force (F_s) must equal (or exceed) f_{sma} (and must do so at deflection $\delta = \delta_0$), we have

$$\frac{Gd^4}{64nr^3}\delta_0 \geqslant \sigma_{\alpha\beta}Bt_f \tag{15}$$

While necessary, Eq. (15) is not sufficient to specify the spring's design; another relation is obtained from the condition that the spring's shear strain limit not be exceeded during compression. The shear strain is given by

$$\gamma_s = \frac{\delta d}{4\pi nr^2} \tag{16}$$

The shear strain limit for spring steel is approximately 1.2%, but in the case of repeated loading (fatigue) this must be reduced somewhat. We assume a limiting shear strain of 1% here. Substituting this into (16) and using $c = r/d$ gives a limiting condition on the maximum deflection, δ_c:

$$\delta_c \leqslant 0.04\pi nc^2 d \tag{17}$$

The maximum deflection given by (17) can be related to δ_0 by noting that the spring's total change in length, $\delta_0 - \delta_c$, must be equal to the contraction of the SMA element of initial length, λ, i.e. $\delta_0 - \delta_c = \varepsilon_{\alpha\beta}\lambda$, where $\varepsilon_{\alpha\beta}$ is the shape memory recovery strain. Combining this with (17) then leads to

$$\delta_0 \leqslant 0.04\pi nc^2 d + \lambda\varepsilon_{\alpha\beta} \tag{18}$$

Substituting into (15) and solving for the spring's wire diameter, d, gives

$$d = \sqrt{\frac{15.61\varepsilon_{\alpha\beta}^2\lambda^2}{c^4n^2} + \frac{510.4t_f c\sigma_{\alpha\beta}}{G}} - \frac{4\varepsilon_{\alpha\beta}\lambda}{c^2 n} \tag{19}$$

Therefore, given the truss design, material properties of the SMA and spring, selection of the number of coils for the spring as well as its ratio of coil radius to wire diameter, (19) gives the minimum wire diameter satisfying the restoring force and failure criteria. According to Eq. (19), the wire diameter decreases monotonically with decreasing values of both c and n, so that the mass of the spring is reduced by selecting smaller values for these two quantities. There is a limit however, to how small the spring can be made; one consideration is that as the spring coil radius decreases relative to spring length (fixed), the spring requires a

guide to prevent it from buckling outward and thus, additional mass. Therefore, to minimize spring mass while hopefully avoiding the need for a spring guide, we choose values of $c = 3$ and $n = 5$.

The mechanical performance of the two actuator designs can now be compared on a unit weight basis. The overall dimensions of the two cantilever beam actuators will be identical and taken to be $H = 8$ mm, $B = 10$ mm and $L = 150$ mm. The truss corrugation angle, θ, is also fixed for both designs at $\theta = \pi/4$. An arbitrary value for the applied tip load is chosen and used with Eqs. (6)–(8) and (11), (12) to determine the appropriate material thicknesses. These are then used to compute the weight index for each design corresponding to the applied load. Finally, the load index (defined as $\Pi = N/(E_{\beta}BL)$) is determined and plotted versus weight index. The result, shown in Fig. 9, indicates that for very low applied loads, the bias design provides the lightest weight solution. However, as the applied load increases, the integral design offers an increasingly significant weight advantage. This is a result of the weight penalty imposed upon the bias design by the spring; while the force capability of the spring scales linearly with wire diameter (for fixed c), its volume (and hence mass) grows with the cube of the wire diameter. It can be seen that for high loads (e.g. $\Pi \geqslant 0.5$), the integral design offers weight savings exceeding 100% in comparison with the bias design.

6. Summary

An integral two-way, shape-reversing structural element (panel, beam) concept has been described, which relies on SMA components exhibiting the one-way shape memory effect. It uses no external bias mechanisms for shape reversal. The concept is based on the incorporation of a lightweight core design exhibiting a combination of very low flexural rigidity and relatively high in-plane stiffness. A prototype structural element (cantilever beam) has been constructed using Ni–Ti SMA face sheets joined to a stainless steel truss core, and tested for shape-reversal and load actuation capacity. Tests of the prototype were able to successfully demonstrate the shape-reversing capability of the design, and characterize its performance. Up to 120 mm displacement over 200 mm span of the beam is achieved experimentally. An analysis of the structural actuator's displacement and load capacity, power consumption and cycling frequency are developed to provide further design guidance. Comparison of the integral reversing actuator concept with a bias-based design also indicates that lighter actuators with higher lift capacity are achievable via the integral design.

Acknowledgements

The authors would like to thank Drs. A.G. Evans, T.J. Lu, N.A. Fleck and J.W. Hutchinson for helpful discussion. Thanks also to Dr. D. Sypeck for help with construction of the actuator core. Funding for this research was provided by the Defense Advanced Research Projects Agency (Dr. Leo Christodolou) and the Office of Naval Research (Dr. Steve Fishman).

References

Allen, H.G., 1969. Analysis and Design of Structural Sandwich Panels. Pergamon Press, Oxford.

Bart-Smith, H., 2001. Private communication.

Baumeister, T., Avallone, E.A., Baumeister III, T. (Eds.), 1978. Marks' Standard Handbook for Mechanical Engineers. McGraw-Hill, New York, pp. 8-76–8-77.

Flomenblit, J., Budigna, N., Bromberg, Y., 1994. Ni–Ti Medical Stent. European Patent No. EP0626153, May 20.

Fu, Y., Huang, W., Du, H., Huang, X., Tan, J., Gao, X., 2001. Characterization of TiNi shape memory alloy thin films for MEMS applications. Surf. Coat. Technol. 145, 107–112.

Garcia, E., 2002. Smart structures and actuators: past, present and future. In: McGowan, A.-M.R. (Ed.), Smart Structures and Materials 2002: Industrial and Commercial Applications of Smart Structures Technologies, Proc. of SPIE, vol. 4698, pp. 1–12.

Gibson, L.J., Ashby, M.F., 1997. Cellular Solids: Structure and Properties, second ed. Cambridge University Press, New York.

Lu, T.J., Hutchinson, J.W., Evans, A.G., 2001. Optimal design of a flexural actuator. J. Mech. Phys. Solids 49 (9), 2071–2093.

Lu, T.J., Evans, A.G., Bart-Smith, H., 2002. Private communication.

Mellor, B.G., 1987. In: Torra, V. (Ed.), The Science and Technology of Shape Memory Alloys, Barcelona, p. 334.

Otsuka, K., Wayman, C.M., 1998. Shape Memory Materials. Cambridge University Press, New York.

Saburi, T., 2000. Shape Memory Materials: Proceedings of the International Symposium on Shape Memory Materials. Trans Tech Publications, Uetikon-Zuerich, Switzerland.

Schetky, L.M., 1998. Engineering applications for shape memory alloys: present status, future potential. In: Intl. Conf. on Displacive Phase Transformations and Their Applications in Materials Engineering. Minerals, Metals and Materials Society/AIME, Warrendale, PA, USA, pp. 149–156.

Srinivasan, A.V., McFarland, D.M., 2001. Smart Structures: Analysis and Design. Cambridge University Press, New York.

Sypeck, D.J., Wadley, H.N.G., 2001. Cellular metal truss core sandwich structures. In: Banhart, J., Ashby, M.F., Fleck, N.A. (Eds.), Cellular Metals and Metal Foaming Technology. MIT Verlag, pp. 381–386.